Article ID 1004-924X(2004)05-0491-13

Highly sensitive micromachined tunneling sensors

XUE Wei, WANG Jing, CUI Tian-hong

Department of Mechanical Engineering, University of Minnesota, Twin Cities 111, *Church Street S E, Minneapolis, MN* 55455, *USA*

Abstract: Highly sensitive silicon micromachined tunneling sensors with small size and light mass have been widely explored in the last 15 years. Many types of tunneling sensors have been developed. This paper presents a review of silicon micromachined tunneling sensors. Four types of tunneling sensors including accelerometers, gyroscopes, infrared sensors, and magnetic sensors are reviewed. Various designs, fabrication procedures, performance, control systems, and noise constraints of silicon tunneling sensors are described and discussed. Novel polymer-based tunneling accelerometers fabricated by PMMA and hot embossing technique are introduced. The structure, fabrication process and characterization of the polymer-based sensor are presented. We can expect that the polymer tunneling sensor has the potential to become the basis for the next generation of highly sensitive MEMS-based sensors in many areas.

Key words: tunneling sensor; sensitivity; resolution; polymer; hot embossing; low frequency noise

基于 MEMS 微加工技术的高灵敏度隧道传感器的研究

薛 伟,王 晶,崔天宏
(美国明尼苏达大学 机械工程系和纳米加工研究中心)

摘要:基于硅加工的高灵敏微型隧道传感器在过去 15 年里得到了充分的发展。多种隧道传感器被开始出来,例如加速度计,角速度计,红外传感器,磁性传感器等。首先对基于硅加工的隧道传感进行了简单的总结。对四种传感器进行了总结和讨论,包括几种器件的结构设计,加工过程,器件性能,控制电路和系统噪音。特别介绍了一种新型的基于高分子聚合物的隧道加速度计,并讨论了其结构,加工与测试,隧道效应得到了进一步验证。同时给出了这种新型高灵敏传感器在很多领域的应用展望。

关 键 词:隧道传感器;灵敏度;分辨率;聚合物;热模压加工;低频噪音
中图分类号:TP212.1 **文献标识码**:A

Received date:2004-03-16; **Revised date**:2004-06-27.

1 Introduction

The theoretical transmission probability of electrons through one-dimensional barrier has been studied in quantum mechanics for more than 60 years. However, since the condition to establish the tunneling current is hard to obtain, it takes many years to develop the real applications of the tunneling mechanism. Quantum electron tunneling effect through vacuum or air barrier was originally developed for microscope applications. Binning and Rohrer developed the first Scanning Tunneling Microscope (STM) by utilizing the tunneling mechanism, and they were awarded the Nobel Prize in 1986[1]. Quantum electron tunneling effect has then been widely studied and developed in many applications after the invention of STM. By utilizing the tunneling current, a variety of highly sensitive microsensors can be fabricated, such as accelerometers[2-4], gyroscopes[5], uncooled infrared sensors[6], magnetic sensors[7-8], etc.

Due to the exponential relationship between the tunneling gap and the tunneling current, the sub-changes of the tunneling gap induce measurable changes in the tunneling current. This high sensitivity is independent of the lateral size of the device due to the extremely small size of the sensing (tip) area. This high sensitivity and miniature size make it possible to fabricate micromachined tunneling sensors with high performance, small size, light mass, and low cost. The highly sensitive tunneling sensors are in great demand in many applications such as seismology, navigation, remote temperature sensing, intrusion detection, and magnetic sensing.

This paper has two parts. First, it presents a brief review of the silicon micromachined tunneling sensors, including accelerometer, gyroscope, uncooled infrared sensor, and magnetic sensor. Various designs, operations, fabrication procedures, performance of the silicon tunneling sensors are reviewed. The feedback control circuits and the noise constraints of the sensors are also briefly described and discussed. After the review, a novel polymer-based tunneling accelerometer is introduced and reviewed. Instead of silicon, an inexpensive polymer material, polymethylmethacrylate (PMMA), was chosen as the structural material. The silicon mold inserts were fabricated by conventional silicon-based micromachining techniques such as UV lithography, wet etching, and dry etching. Hot embossing technique was used to produce the polymer structure. Mass production is readily achieved by hot embossing and polymer materials. With simple feedback control circuit, wide-bandwidth, high-sensitivity and high-resolution sensors were successfully developed and characterized. Polymer-based tunneling sensors therefore exhibit great promise as an inexpensive, highly sensitive sensing platform for biosensing applications.

2 Silicon-based tunneling sensors

2.1 Tunneling accelerometer

Among all the MEMS devices, accelerometers have the second largest volume after pressure sensors[9]. The detection of acceleration relies on the classical Newton's mechanics. In other words, when the device is accelerated, the proof mass is displaced due to the inertial force. The tunneling current through the electrodes varies exponentially with the change of the tunneling gap. The acceleration can be recorded by reading out the deflection voltage in the feedback control circuit. Compared with other common and well developed accelerometers such as capacitive, piezoresistive, and piezoelectric accelerometers, the tunneling accelerometer can achieve higher sensitivity and higher resolution with smaller size and lighter mass. The main disadvantage of the tunneling accelerometer is the relatively complicated fabrication process.

The tunneling accelerometer was first introduced by S. B. Waltman and W. J. Kaiser at Jet

Propulsion Laboratory and California Institute of Technology[10]. Since then, several groups have developed different types of tunneling accelerometers. In general, there are two kinds of accelerometers: vertical accelerometers and lateral accelerometers. Vertical tunneling accelerometer is sensitive to Z-axis acceleration which is normal to the wafer surface. Lateral tunneling accelerometer is sensitive to X- or Y-axis acceleration which is parallel to the wafer surface. Basically, the vertical tunneling accelerometer can be divided into two groups: membrane-based[11] and cantilever-based accelerometers, as shown in Fig. 1[2][12]. These devices are fabricated by standard silicon bulk- or surface-micromachining techniques such as UV lithography, wet etching, sputtering, low pressure chemical vapor deposition (LPCVD), lift-off, etc.[3-4][13-14] The tunneling tips can be fabricated by KOH etching[2] and focused ion beam milling[3]. The main advantages of the cantilever structure are larger linearrange and higher sensitivity. The main advantage of the membrane structure is easy to be fabricated and assembled.

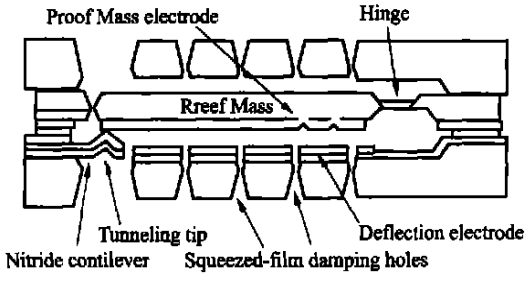

(a) Developed at Stanford University[2]

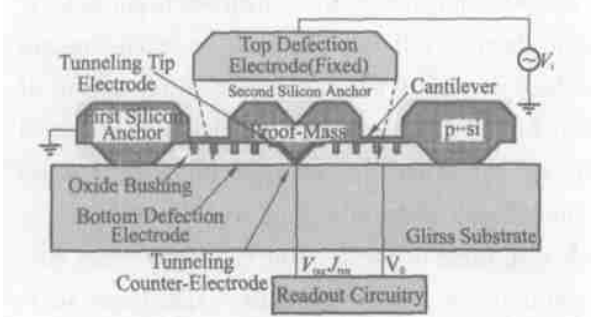

(b) Developed at University of Michigan[12]

Fig. 1 Cross section of cantilever-based tunneling accelerometers

C. H. Liu and T. W. Kenny at Stanford University reported a high-precision, wide-bandwidth silicon bulk-micromachined tunneling accelerometer (as shown in Fig. 1a) with a high resolution of 20 ng/ Hz (1 g = 9.8 m/ s^2), sensitivity of 0.44 V/ mg, and a bandwidth of 5 Hz-1.5 kHz[2]. High deflection voltage is required for these devices to set the operation point. From another report, the mean operation voltage is about 41 V and the standard deviation is 2 V[13]. However, the operation voltage exceeded 300 V in several hand-assembled devices. Chingwen Yeh and Khalil Najafi at University of Michigan developed a low-voltage silicon bulk-micromachined tunneling accelerometer (as shown in Fig. 1b) with CMOS interface circuity[15]. Only one power supply of 10 V is required for device operation, and the total power dissipation is as low as 2.5 mW. This device has a sensitivity of 125 mV/ g, bandwidth of 2.5 kHz, resolution range from 4 mg/ $\sqrt{\text{Hz}}$ (at 0.5 Hz) to 0.1 mg/ $\sqrt{\text{Hz}}$ (at 2.5 kHz), and dynamic acceleration measurement range of 30 g (- 20 g to 10 g). R. L. Kubena and his coworkers at Hughes Research Laboratory fabricated a tunneling accelerometer using surface micromachining techniques[3][16]. The tunneling tip is defined by Focused Ion Beams (FIB) lithography and ion milling. The accelerometer has a noise level resolution of 8.5×10^{-5} g/ $\sqrt{\text{Hz}}$ at 500 Hz and its dynamic acceleration measurement range is over 10^4 g.

In general, bonding techniques are required in the design of silicon bulk-micromachined vertical tunneling accelerometers. Several micromachined wafers are bonded together to construct the whole device. Due to the variation from the fabrication and bonding process, the parameters of the accelerometer vary from device to device. To overcome this disadvantage, lateral tunneling accelerometers were developed as well[17-18]. The variation of the tunneling gap and the tunneling

current is caused by the lateral acceleration. The device characteristics can be precisely controlled by simple micromachining techniques to match the specific applications. Devices can be specifically designed to meet the requirements of resolution, sensitivity, and bandwidth. P. G. Hartwell at Cornell University reported a single mask lateral tunneling accelerometer with a high resolution of 20 μg/ Hz at 100 Hz, high sensitivity of 0.23 V/g, and a wide bandwidth of 55 kHz. As shown in Fig. 2[18], the proof mass is supported by several beams, and high-aspect-ratio comb-drive structures are used as the electrostatic actuators. The comb-drive actuators are designed to provide sufficient electrostatic force to set the operation point, and provide self-test acceleration excitations with different ranges.

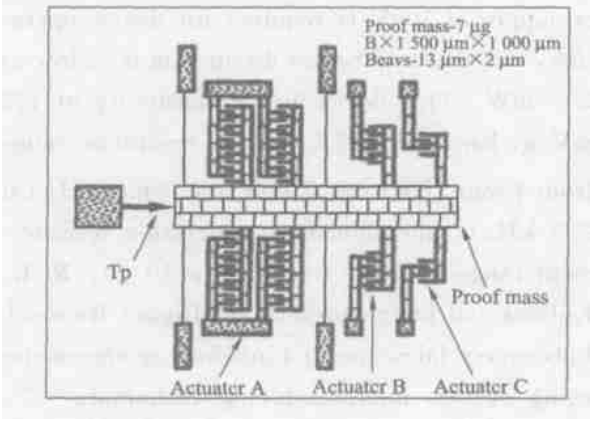

Fig. 2 (a) Schematic of a lateral tunneling accelerometer

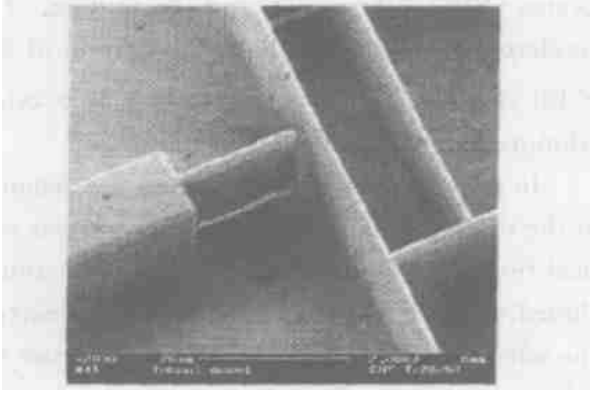

Fig. 2 (b) SEM image of integrated tip and proof mass[18]

2.2 Tunneling gyroscope

Micromachined tunneling gyroscopes for inertial rotation rate measurements were designed and fabricated by R. L. Kubena and his coworkers at Hughes Research Laboratories[5]. The tunneling gyroscope is based on the Coriolis Effect described elsewhere[9]. A top view image of the tunneling gyroscope is shown in Fig. 3[19]. The structures are fabricated by silicon surface-micromachining techniques. A Ni cantilever beam, located above a tunneling tip, is driven at its resonant frequency in the horizontal direction which is parallel to the surface of the substrate. The tunneling current between the tip and the cantilever beam is sensitive to the Coriolis force in the vertical direction which is normal to the substrate. Due to the high sensitivity of the tunneling mechanism, precise mechanical tuning of the drive is not required.

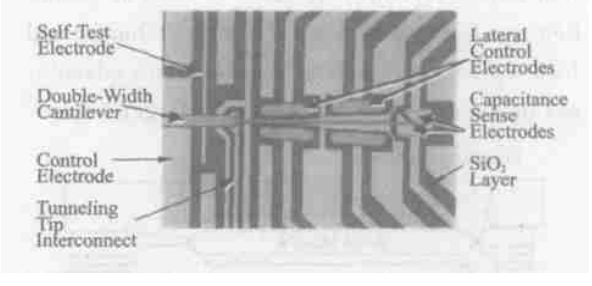

Fig. 3 Top view image of tunneling gyroscope[19]

As shown in Fig. 3, the dimension of the Ni cantilever is 2 μm thick, 100 μm long in the wide portion and 200 μm in the narrow portion. The wide portion of the cantilever beam is located above a self-test electrode, a tunneling tip which is used to detect the vertical movement of the beam, and a control electrode which is used to set the tunneling operation position. Lateral control electrodes are employed to provide the driving force to oscillate the cantilever beam horizontally. A pair of triangular capacitance sensing electrodes, which is underlying the far-end of the cantilever beam, is used to detect the horizontal movement of the cantilever beam. The interface circuit to control the horizontal and the vertical movement of the cantilever

beam was designed[5]. The circuit consists of two servo control loops, which are used for horizontal and vertical sensing and maintenance, respectively. The horizontal servo senses the capacitance through the electrodes and maintains the beam oscillating at its resonant frequency. The vertical servo senses the tunneling current and maintains the tunneling operation position. The final analog rate signal can be measured by recording the output of the vertical servo. A 27 °/h/ Hz noise floor was demonstrated by a tunneling gyroscope with a 300 μm-long cantilever beam.

2.3 Tunneling uncooled infrared sensor

Uncooled infrared sensors have been widely used in low-cost applications such as remote temperature sensing, intrusion detection, night operation, etc.[20-21] In general, uncooled infrared sensors are based on thermal detection principles. Thermal detectors are employed in the infrared sensing systems. At room temperature, Golay Cell-based infrared detector offers the highest sensitivity, compared with other infrared detectors such as bolometer-based, Pyroelectric-based and thermopile-based infrared detectors[22]. As originally designed, the Golay Cell had a fragile membrane and a gas cell. The gas in the Golay Cell is heated due to the absorption of the infrared radiation. The gas expands thermally and forces the membrane to deflect outwards. Optical beams and capacitive displacement transducers are normally used techniques to detect the deflection of the membrane[23]. Tunneling-based transducers can also be used to detect the deflection of the membrane. The extremely high sensitivity of the tunneling transducer enables the development of miniature, robust, and high performance infrared sensors.

Researchers at Stanford University developed the silicon bulk-micromachined tunneling infrared sensor[24-25]. As shown in Fig. 4[26], the cross section of the tunneling infrared sensor is similar to the vertical accelerometer. The difference is that the infrared sensor has another (top) wafer mounted on the middle wafer. Golay Cell is constructed by bonding the top two wafers. A pinhole in the top membrane[6] or a lateral leak channel on the bonding ring[13] can be formed to minimize the DC response of the sensor. A thin layer of platinum (about 40 Å) is deposited on top of the silicon nitride membrane as the infrared absorber. The advantages of the platinum over other metals such as aluminum and gold are that platinum has relatively high conductivity, and that it is controllable and very stable during the evaporation. Both the top two wafers and the tunneling tip structure are fabricated by KOH wet etching technique. Corrugations can be fabricated in the lower sensing membrane to extend the linear range of the membrane deflection. Gold is used as the electrode material in the membrane electrode, deflection electrode, and the tunneling tip electrode. Tunneling infrared sensors with the different membrane structures were developed at Stanford University. The measured infrared sensitivity, signal-noise ratio (SNR), and the noise equivalent power (NEP) of the membrane-based tunneling infrared sensor are 125 kV/W, 27/ $\sqrt{\text{Hz}}$, and 3×10^{-10} W/ $\sqrt{\text{Hz}}$ (at 47 Hz), respectively[6], which show the best performance among all the uncooled infrared sensors with similar dimensions[21].

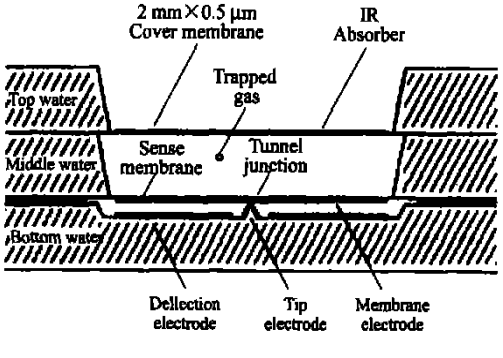

Fig. 4 Structure of tunneling infrared sensor[26]

S. S. Lee and his coworkers in Japan developed a bimetallic cantilever-based uncooled infrared sensor using the tunneling transducer[27]. A 600 nm-thick NiCr (80:20) layer is coated on the cantilever beam by sputtering. When absorbing infrared radiation, the NiCr layer causes the cantilever beam to bend due to the thermal bimetallic effect. The displacement of the cantilever beam is detected by a tunneling displacement transducer. The measured noise level is 35 μV/ Hz at 10 Hz, the calculated signal-noise ratio (SNR) is 14.3×10^3/ $\sqrt{\text{Hz}}$ at 10 Hz, and the noise equivalent power (NEP) is given as 35×10^{-10} W/ Hz at 10 Hz and $24.4 10^{-10}$ W/ Hz at 30 Hz.

2.4 Magnetic tunneling sensor

Magnetic tunneling magnetic sensors, or magnetometers, have also been developed based on electron tunneling mechanism. The first tunneling magnetic sensor was reported by J. H. Wandass et al. in 1989[8]. A tunneling transducer was used to measure dimensional changes of an amorphous Fe-B-Si magnetostrictive ribbon when it is exposed to an external DC or AC magnetic field. The reported resolution of this magnetometer is 2000 nT at 1 Hz. A resolution of 6 nT/ $\sqrt{\text{Hz}}$ at 1 Hz and further discussion of the magnetic sensor were reported in their later papers[28-31]. Fig. 5 shows the schematic diagram of the tunneling magnetic sensor including four main parts: the tunneling tip, the feedback electronics, the solenoid coil, and the magnetostrictive ribbon.

Magnetic tunneling magnetic sensors with different structures have been developed. L. M. Miller et al. at Jet Propulsion Laboratory (JPL) reported a μ-magnetometer based on the vertical tunneling sensor structure[32]. A wire coil loop is fabricated on the membrane. The membrane can detect the change of the Lorentz Force produced by the interaction between the magnetic field and the current through the coil loop. The measured noise resolution is about 6 μT/ $\sqrt{\text{Hz}}$. By changing the parameters of the magnetometer, a noise resolution of 4 nT/ $\sqrt{\text{Hz}}$ is achievable. D. DiLella et al. developed a silicon bulk-micromachined magnetic tunneling sensor with a torsion element[7]. A torsion arm senses the magnetic field and rotates around its pivot points. Neodymium-iron-boron is coated on the torsion arm as the magnet. The size of the rectangular-shaped magnet is about $9 \times 4 \times 0.5$ mm^3 and the mass is about 150 mg. The calculated noise resolution is 0.002 nT/ Hz at 1 Hz and the measured noise resolution is 0.3 nT/ $\sqrt{\text{Hz}}$ at 1 Hz. As summarized by D. DiLella, the comparison of tunneling magnetic sensor with other related sensors shows that the tunneling-based sensor has relatively small size (10 cm^3) and low power dissipation (1 mW)[7].

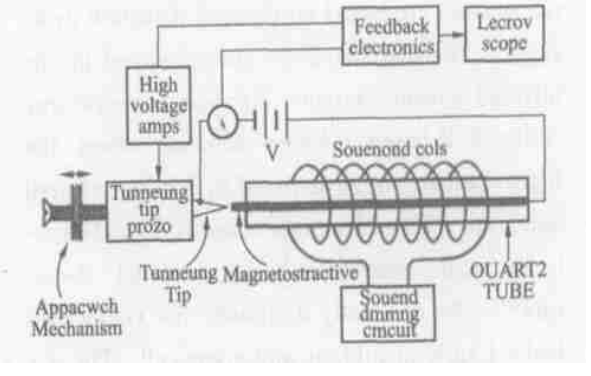

Fig. 5 Schematic diagram of the tunneling magnetometer[30]

2.5 Feedback control circuitry

To improve the performance and enlarge the dynamic measurement range, tunneling sensors usually are operated in a close-loop mode. Several mathematical models were developed to describe the tunneling mechanism and the feedback circuit[15][33]. As shown in Fig. 6[15], the block diagram of the closed-loop sensor-circuit system contains four blocks: a suspended proof mass, a tunneling-based mechanism block, a current-to-voltage amplifier, and an electrostatic feedback actuator.

Compared with the interface circuits of other

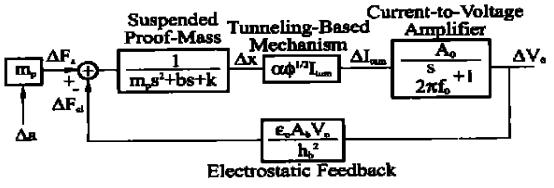

Fig. 6 Block diagram of closed-loop tunneling sensor-circuit system[15]

accelerometers such as capacitive and piezoresistive accelerometers, the feedback control circuit of the tunneling accelerometers is much simpler. Circuits with discrete components such as resistors, capacitors, and amplifiers have been widely used in the tunneling sensor systems, as shown in Fig. 7[11-12].

The integrated control circuits are preferred for most MEMS devices. Monolithic or hybrid integration can effectively reduce the cost of the whole system, lower the power dissipation, and improve the device resistance to external environments. Complementary metal-oxide-semiconductor (CMOS) based feedback circuits have also been designed and fabricated in different research institutions. Chingwen Yeh and Khalil Najafi reported a hybrid sensor-circuit integration method by using three CMOS interface circuitry for tunneling accelerometers. Only one power supply of 10 V is required for device operation, the total dissipation reaches 2.5 mW[14]. The exponential relationship between the tunneling current and the tunneling gap is linearized by a PN-junction diode. Thus, the output voltage is linearly proportional to the external acceleration. Aaron Partridge and his coworkers developed an integrated controller for tunneling sensors which provides all necessary control functions[26]. The tunneling current/gap exponential relationship is linearized by a diode-connected transistor. Two power supplies (-5 V and -40 V) are required for device operation, and the total power dissipation is about 0.9 mW.

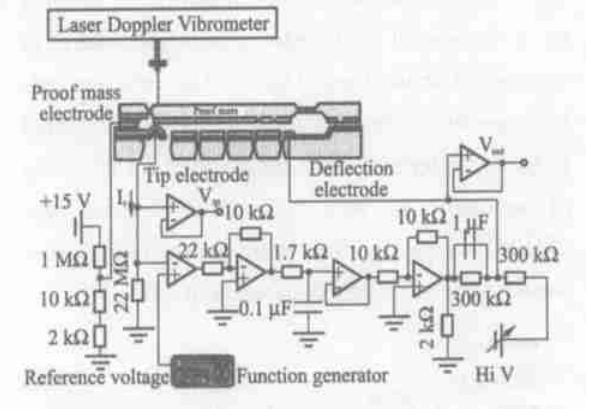

Fig. 7 Tunneling accelerometer system with simple feedback control circuit composed of several discrete components[11]

2.6 Noise constraints

One disadvantage of the tunneling sensors is their high low-frequency noise level[2] [14] [34]. The main noise sources of the tunneling sensors include thermo-mechanical noise caused by thermal agitation and energy dissipation, 1/f mechanical noise caused by package relaxation and thermal creep, bimorph effect caused by thermal expansion mismatch between different materials, drift in the work function of the electrode material, and 1/f tunneling noise observed in tunneling sensors. 1/f tunneling noise, though has not been well understood, was proved to be the dominant noise source at most frequencies. The possible factors that may contribute to 1/f noise include migration of atoms, interactive atomic force, and mobile adsorbed contamination. The total noise level of the device can be reduced by modifying the design of the structures.

3 Polymer-based tunneling accelerometer

For most MEMS devices, especially precision MEMS and devices need integrated electronics, silicon is the dominant material. However, since the application areas have been broadened, polymers are becoming more and more important as low-cost

alternatives to silicon or glass. Hot embossing technique provides an inexpensive and high-volume polymer microfabrication method on a variety of materials to produce micro to nano-scale structures. Due to the inherent advantages of the hot embossing and the associated polymer materials, they can be used for a variety of applications, such as optical devices, BioMEMS, microfluidics, high-aspect-ratio structures, nano-scale resist patterning, etc. [35-37]

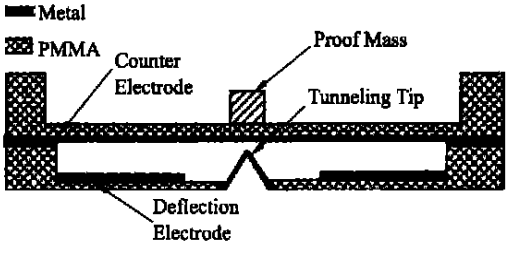

Fig. 8 Cross section of membrane-based tunneling accelerometer[38]

To explore the tunneling sensor technology, polymers, and polymer fabrication techniques, all polymer-based vertical tunneling accelerometers were fabricated and characterized in our lab[38-39]. A typical tunneling accelerometer consists of mechanical components and three electrodes. Since membrane structures are easier to be fabricated and assembled, and it is more suitable for hot embossing technique, we choose membrane as the sensing mechanical component. The cross section of a membrane-based vertical tunneling accelerometer is illustrated in Fig. 8. The mechanical components comprise a substrate with a tunneling tip and a membrane with a proof mass. The electrodes include a tunneling tip electrode, a counter electrode on the backside of the membrane, and a deflection electrode. Gold is chosen as the electrode material due to its inert chemical characteristics as well as its relatively high work function.

All the mechanical structures of the PMMA tunneling accelerometer were fabricated by hot embossing technique. Silicon molds are the key factors to reproduce the structures by hot embossing. The reason is that if we can strictly control the fabrication condition, there is almost no feature size loss during the pattern replication. By using well-developed silicon molds with sharp angles and smooth surfaces, the sensor structures can be easily replicated within 20 minutes. In order to meet the requirements for different components of the sensor, a combination method of KOH (potassium hydroxide) etching and plasma ion etching was used to construct the silicon mold insert.

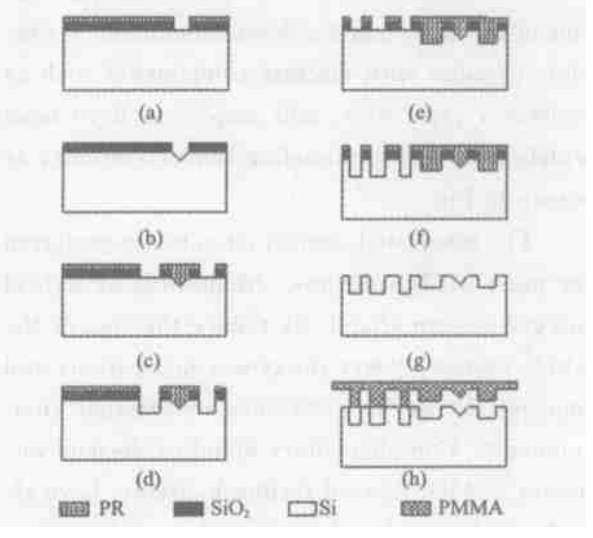

Fig. 9 Fabrication process for silicon mold by hot embossing lithography

Double polished (100) orientation silicon wafers coated with 2 μm thermal oxide layer were selected for the mold inserts. A layer of positive photoresist (PR1813) was spin coated on the silicon wafer and patterned by UV lithography. The SiO_2 layer was etched by BHF (buffered hydrofluoric acid) (Fig. 9a). The photoresist was removed by acetone and the whole wafer was submerged into a 45 wt % KOH etchant. The etchant was heated at 80 ℃ with a stirrer rotating at 200 rounds per minute (rpm). The etching time is about 60 minutes with an etching rate of 0.8 μm/min (Fig. 9b). Following that, another BHF etching was performed after a second lithography (Fig. 9c). The pyramid pit was then protected thoroughly. A modified Induct Coupled Plasma (ICP) dry etching

process was used, in which SF_6, O_2 and C_4F_8 are used simultaneously to acquire the positive sidewall profiles and a smooth surface. The depth of the sidewall is about 55 μm (Fig. 9d). After the first ICP, the wafer was cleaned and another lithography and BHF etching were carried out (Fig. 9e). The thickness of PR1813 is relatively thicker since the second ICP etched height is about 80 to 100 μm (Fig. 9f). Subsequently, the thermal oxide was removed and the silicon mold insert was thoroughly cleaned (Fig. 9g), which thereby was boned to the Pyrex glass by anodic bonding. The hot embossing lithography was executed and the structures were transferred into PMMA (Fig. 9h). The PMMA was then sliced into two parts, patterned with electrodes separately and assembled together thereafter.

SEM pictures of the fabricated structures are shown in Fig. 10. Fig. 10(a) shows a SEM image of a silicon pit on the mold insert. The sidewalls of the pyramid pit are smooth and the four edges are sharp. Fig. 10(b) shows a replicated PMMA pyramid tip with smooth surfaces, sharp tip point, and steep edges, which can compete with any tunneling tips fabricated by micromachining on silicon.

Similar to traditional silicon-based electrode fabrication techniques, metal layers of Ti/Au (300 Å/1000 Å) are sputtered on PMMA structures and patterned by I_2/KI solution (to pattern Au) and BHF etching (to pattern Ti). The optical photograph of patterned electrodes on tunneling tip part is shown in Fig. 11(a). Instead of typical wire bonding method, conductive silver epoxy is used to bond the wire onto the electrodes. The epoxy bonding shows good results on both mechanical and electrical performances. After the two parts of PMMA structures glued together, it is mounted onto an 18-pin IC socket, as shown in Fig. 11(b).

The tunneling effect was verified when tunneling accelerometer operated at open-loop status. As an ac voltage applied on the deflection elec-

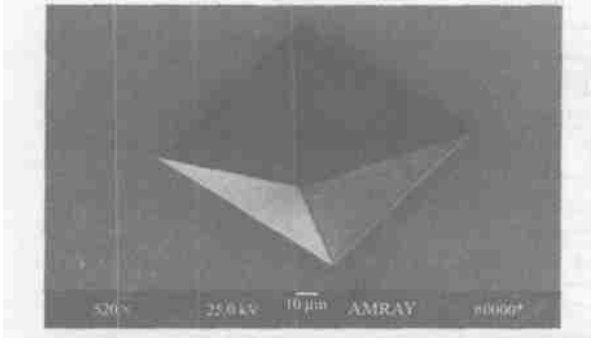

Fig. 10 (a) SEM image of a pyramid pit on silicon mold

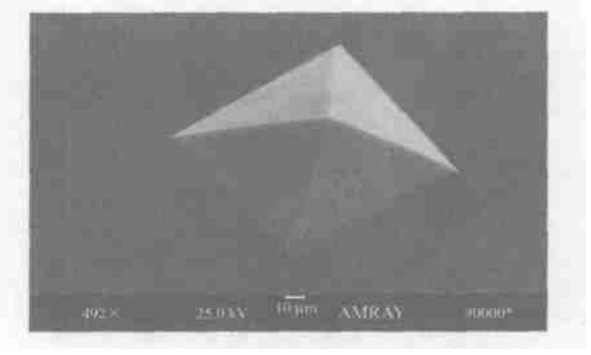

Fig. 10 (b) PMMA pyramid tip

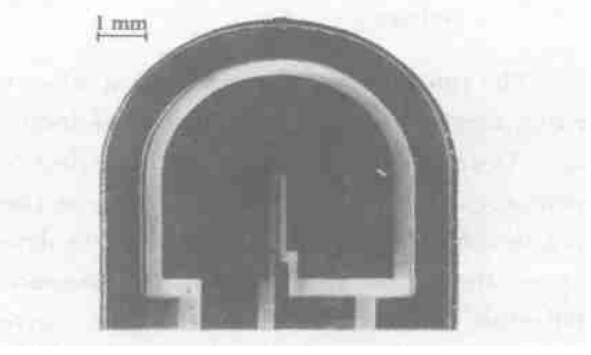

Fig. 11 (a) Optical photograph of patterned electrodes on PMMA structure

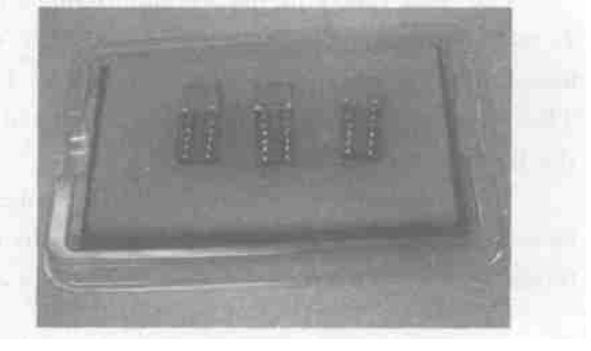

Fig. 11 (b) Assembled PMMA tunneling accelerometers

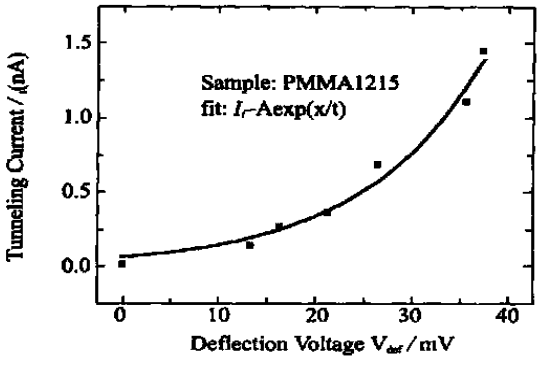

Fig. 12　Measured tunneling current vs deflection voltage

trode , an ac current I_t was induced on tunneling tip. As shown in Fig. 12 , the curve demonstrates the exponential relationship between the deflection voltage and the tunneling current. The open-loop frequency response of a PMMA tunneling accelerometer is shown in Fig. 13(a) .

The peak refers to the natural frequency of f_0 = 128 Hz. The closed-loop bandwidth was measured as B = 6.3 kHz , as shown in Fig. 13b. The frequency range was greatly broadened by the feedback control circuit.

Table 1 shows a comparison of four silicon-based tunneling accelerometers developed by different research groups. The performance of a polymerbased tunneling accelerometer devel-oped in our group is also shown in the table[40]. Most parameters of the polymer-based tunneling sensor are better than or at the same order in magnitude as the silicon-based tunneling sensors.

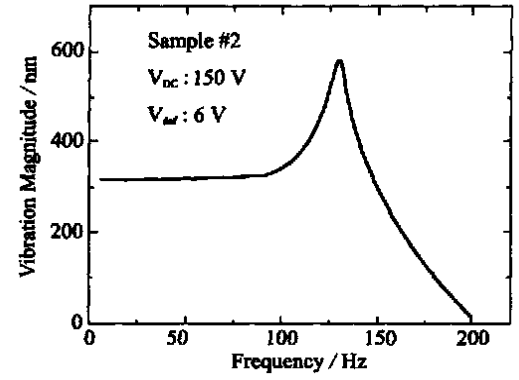

(a) Open-loop system

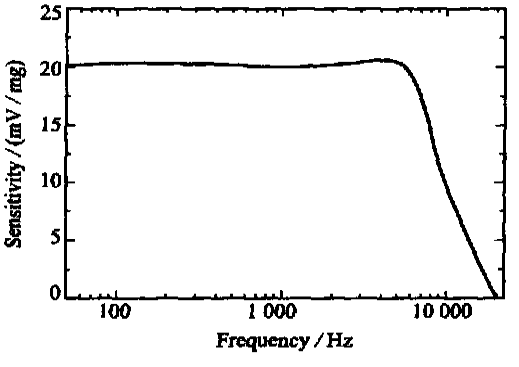

(b) Closed-loop system

Fig. 13　Frequency responses of PMMA tunneling accelerometer

Tab. 1　Comparison of different tunneling accelerometers[2-3],[12],[18],[40]

Properties	Our Group	Stanford University	University of Michigan	Hughes Research Lab	Cornell University
Sensor type	Vertical	Vertical	Vertical	Vertical	Lateral
Structure	Membrane	Cantilever	Cantilever	Cantilever	Comb drive
Fabrication	Polymer-based	Silicon bulk-micromaching	Silicon bulk-micromaching	Silicon surface-micromaching	Silicon surface-micromaching
Natural frequency	133 Hz	100 Hz	640 Hz	71 kHz	4.6 kHz
Tunnel barrier height	0.1685 eV	0.212 eV	0.368 eV	0.05 - 0.2 eV	0.006 eV
Resolution	0.25 μg/ $\sqrt{Hz}$	0.4 μg/ $\sqrt{Hz}$	0.1 mg/ $\sqrt{Hz}$	85 μg/ $\sqrt{Hz}$	20 μg/ $\sqrt{Hz}$
Dynamic range	- 1.5 mg to 1.5 mg	0 - 1 mg	- 20 to 10 g	over 10^4 g	N/A
Sensitivity	26 V/ g	44 V/ g	133 mV/ g	7.9 mV/ g	0.23 mV/ g
Bandwidth	6.3 kHz	1.5 kHz	2 kHz	500 Hz	4.6 kHz

4 Conclusion

Sensors based on quantum electron tunneling effect have been investigated and developed in the past 15 years. Due to the exponential relationship between the tunneling current and the tunneling gap, tunneling sensors are easier to achieve higher sensitivity, compared with other types of sensors. The highly sensitive silicon micromachined tunneling sensors with small size, light mass, and low cost are in great demand in many applications such as seismology, navigation, remote temperature sensing, and intrusion detection.

Four types of tunneling sensors: accelerometer, gyroscope, infrared sensor, and magnetic sensor are reviewed in this paper. For each type, this paper describes the basic structure, operation principle, fabrication method, and performance. Tunneling sensors are recommended to operate in closed-loop systems, which can improve the performance and enlarge the dynamic measurement range. A mathematical model of the system is shown in the paper. Circuits with discrete components can simplify the design of the feedback control system. Monolithic or hybrid integrated control circuit can effectively reduce the cost of the whole system, lower the power dissipation, and improve the device resistance to external environments. For tunneling sensors, the low frequency noise is a problem. Though the tunneling transducer noise has not been well understood, the total noise level can be reduced by modifying the structure of the device.

Novel polymer-based vertical tunneling accelerometers were designed, fabricated, and measured. Hot embossing technique was used to produce inexpensive, high-volume PMMA structures. The silicon mold inserts were fabricated using conventional UV lithography, wet etching, and ICP dry etching techniques. Silicon structures with smooth surfaces and steep angles are shown in the paper. The tunneling effect, the exponential relationship between tip current and applied deflection voltage, was proved. The natural frequency of the tunneling accelerometer is 128 Hz. The bandwidth of the closed-loop system is up to 6.3 kHz.

Tunneling sensors have a wide range of applications. However, they have the constraints of the tunneling noise, especially in the low frequency range. One possible method to overcome the low frequency noise is to apply a high frequency vibrating signal on the sensor structure (cantilever or membrane). Therefore, the low frequency signal (such as gas sensing, DNA sensing signal, etc.) can be modulated to high frequency range. After reducing the low frequency tunneling noise, more devices can be realized, such as gas sensors, chemical sensors, biosensors, etc.

参考文献:

[1] BINNING G, ROHRER H. Scanning tunneling microscopy, an atomic probe[C]. *Scanning Electron Microscopy, Proceeding of the Annual Scanning Electron Microscope Symposium*, 1983: 1079-1082.

[2] LIU C H, KENNY T W. A high-precision, wide-bandwidth micromachined tunneling accelerometer[J]. *Journal of Microelectromechanical Systems*, 2001, 10(3): 425-433.

[3] KUBENA R L, ATKINSON D M, ROBINSON W P, *et al*. A new miniaturized surface micromachined tunneling accelerometer[J]. *IEEE Electron Device Letters*, 1996, 17(6): 306-308.

[4] LIU C H, BARZILAI A M, REYNOLDS J K, *et al*. Characterization of a high-sensitivity micromachined tunneling accelerometer with micro-g resolution[J]. *Journal of Microelectromechanical System*, 1998, 7(2): 235-244.

[5] KUBENA R L, VICKERS-KIRBY D J, JOYCE R J, *et al*. New tunneling-based sensor for inertial rotation rate measurements[J]. *Sensors and Actuators, A: Physical*, 2000, 83(1): 109-117.

[6] KENNY T W, REYNOLDS J K, PODOSEK J A, *et al*. Micromachined infrared sensors using tunneling displacement

transducers[J]. *The Review of Scientific Instruments*, 1996, 67(1): 112-128.

[7] DILELLA D, WHITMAN L J, COLTON R J, *et al*. A micromachined magnetic-field sensor based on an electron tunneling displacement transducer[J]. *Sensors and Actuators, A: Physical*, 2000, 86(1-2): 8-20.

[8] WANDASS J H, MURDAY J S, COLTON R J. Magnetic field sensing with magnetostrictive materials using a tunneling tip detector[J]. *Sensors and Actuators*, 1989, 19: 211-225.

[9] NAVID Y, FARROKH A, KHALIL N. Micromachined inertial sensors[C]. *Proceedings of the IEEE*, 1998, 86(8): 1640-1659.

[10] WALTMAN S B, KAISER W J. An electron tunneling sensor[J]. *Sensors and Actuators*, 1989, 19: 201-210.

[11] LIU C H, REYNOLDS J K, PARTRIDGE A, *et al*. High-bandwidth feedback control of micromachined tunneling sensors[C]. *Proceedings of the ASME Dynamic Systems and Control Division*, 1995: 1001-1010.

[12] CHINGWEN Y, KHALIL N. *A low-voltage bulk-silicon tunneling-based silicon microaccelerometer*[M]. Technical Digest - International Electron Devices Meeting, 1995: 593-596.

[13] GRADE J, BARZILAI A, REYNOLDS J K, *et al*. Wafer-scale processing, assembly, and testing of tunneling infrared detectors[C]. 1997 *International Conference on Solid-State Sensors and Actuators, Chicago*, 1997: 1241-1244.

[14] CHINGWEN Y, KHALIL N. A low-voltage tunneling-based silicon microaccelerometer[J]. *IEEE Transactions on Electron Devices*, 1997, 44(11): 1875-1882.

[15] CHINGWEN Y, KHALI N. CMOS interface circuity for a low-voltage micromachined tunneling accelerometer[J]. *Journal of Microelectromechanical Systems*, 1998, 7(1): 6-15.

[16] KUBENA R L, ATKINSON G M, ROBINSON W P, *et al*. A new high-performance surface-micromachined tunneling accelerometer fabricated using nanolithography[J]. *Journal of Vacuum Science & Technology B: Microelectronics Processing and Phenomena*, 1996, 14(6): 4029-4033.

[17] DAI K, TOSHIKI H, TOMOTAKE F, *et al*. An integrated lateral tunneling unit[C]. *Proceeding of IEEE Micro Electro Mechanical Systems Workshop*, 1992: 214-219.

[18] HARTWELL P G, BERTSCH F M, MILLER S A, *et al*. Single mask lateral tunneling accelerometer[C]. *Proceedings of the* 1998 *IEEE* 11*th Annual International Workshop on Micro Electro Mechanical Systems*, 1998: 340-344.

[19] KUBENA R L, VICKERS-KIRBY D J, JOYCE R J, *et al*. A new tunneling-based sensor for inertial rotation rate measurements[J]. *Journal of Microelectromechanical Systems*, 1999, 8(4): 439-447.

[20] WILLARDSON R K, BEER A C. *Semiconductors and semimetals*[M]. Infrared Detectors, Academic Press, 1970

[21] KRUSE P W, SKATRUD D D. *Semiconductors and semimetals*[M]. Uncooled Infrared Imaging Arrays and Systems, Academic Press, 1997.

[22] GOLAY M J E. Theoretical consideration in heat and infra-red detection, with particular reference to the Pneumatic Detector[J]. *The Review of Scientific Instruments*, 1947, 18(5): 347-356.

[23] GOLAY M J E. A Pneumatic Infra-Red Detector[J]. *The Review of Scientific Instruments*, 1947, 18(5): 357-362.

[24] KENNY T W, KAISER W J, WALTMAN S B, *et al*. Novel infrared detector based on a tunneling displacement transducer[J]. *Applied Physics Letters*, 1991, 59(15): 1820-1822

[25] KENNY T W, KAISER W J, PODOSEKJ A, *et al*. *Micromachined electron tunneling infrared sensors*[M]. Technical Digest-IEEE Solid-State Sensor and Actuator Workshop, 1992: 174-177.

[26] PARTRIDGE A, REYNOLDS J K, GRADE J D, *et al*. An integrated controller for tunnel sensors[J]. *Journal of Microelectromechanical Systems*, 1999, 34(8): 1099-1107.

[27] SEUNG S L, TAKAHITO O, KAZUHIRO N. Electrostatic servo controlled uncooled infrared transducer[J]. *Sensors and Actuators*, 2000, 12(5): 301-314.

[28] BRIZZOLARA R A, COLTON R J, WUN-FOGLE M, *et al*. A tunneling-tip magnetometer[J]. *Sensors and Actuators*, 1989, 20: 199-205.

[29] BRIZZOLARA R A, COLTON R J. Magnetostriction measurements using a tunneling-tip strain detector[J]. *Journal of Magnetism and Magnetic Materials*, 1990, 88: 343-350.

[30] BRIZZOLARA R A, COLTON R J. The magnetostriction of CoFeNiMo metallic glasses measured with a tunneling transducer[J]. *Journal of Magnetism and Magnetic Materials*, 1992, 103: 111-116.

[31] WITEK A, ONN D G. Proposal for a novel magnetometer[J]. Journal of Vacuum Science and Technology, 1991, 9: 639-642.

[32] MILLER L M, PODOSEK J A, KRUGLICK E, *et al*. A μ-magnetometer based on electron tunneling[C]. *Proceedings of the IEEE Microelectromechanical Systems (MEMS)*, 1996: 467-472.

[33] LIU C H, ROCKSTAD H K, KENNY T W. Robust controller design via μ-Synthesis for High-performance micromachined tunneling accelerometers[C]. *Proceeding of the American Control Conference, San Diego, California*, 1999, 4: 247-252.

[34] JOHN G, AARON B, REYNOLDS J K, *et al*. Low frequency drift in tunnel sensors[C]. *International Conference on Solid-State Sensors and Actuators, Chicago*, 1997, 4: 16-19.

[35] HOLGER B, U1F H. Hot embossing as a method for the fabrication of polymer high aspect ratio structures[J]. *Sensors and Actuators, A: Physical*, 2000, 8(1): 130-135.

[36] MARC J, MADOU L, JAMES L, *et al*. Design and fabrication of CD-like microfluidic platforms for diagnostics: microfluidic functions[J]. *Biomedical Microdevices*, 2001, 3(4): 245-254.

[37] LEE G B, CHEN SH H, HUANG G R, *et al*. Microfabricated plastic chips by hot embossing methods and their applications for DNA separation and detection[J]. *Sensors and Actuators, B: Chemical*, 2001, 75(1-2): 142-148.

[38] WANG J, XUE W, CUI T H. A combinative technique to fabricate hot embossing master for PMMA tunneling sensors [J]. *Microsystem Technologies*, 2004, 10(4): 329-333.

[39] WANG J, ZHAO Y J, CUI T H, *et al*. Synthesis of the modeling and control systems of a tunneling accelerometer using the MatLab simulation[J]. *Journal of Micromechanics and Microengineering*, 2002, 12(6): 730-735.

[40] WANG J. *Vertical polymer tunneling sensor platform by hot embossing technique*[D]. Ph. D. Dissertation, Institute for Micromanufacturing, Louisiana Tech University, 2003.

作者简介:薛伟,现为美国明尼苏达大学双城分校机械工程系博士研究生。分别于 1997 年与 2000 年在山东大学电子工程系获得理学学士及工学硕士学位。2001 年至 2003 年在美国路易斯安那理工大学博士研究生。目前主要研究方向包括微米与纳米加工、微机电系统器件等。

王晶,现为美国宾州大学机械系博士后。分别于 1993 年和 1996 年获南开大学电子科学系学士和硕士学位。1999 年获得中国科学院物理研究所博士学位。2003 年获美国路易斯安娜理工大学获电子工程博士学位。主要研究方向是微电子机械系统,生物微流体动力学、生物微米/纳米系统。主要研究成果有:基于全塑材料的微隧道传感器平台,基于全塑材料的 PCR 放大检测系统,和取样于口腔样品的 HIV 病毒,抗体,DNA,RNA 全功能检测系统。

崔天宏,现任美国明尼苏达大学纳米中心和机械工程系 NELSON 讲席副教授。同时,现为 IEEE 资深会员,中国科学院长春光学精密机械与物理研究所兼职教授,大连理工大学特聘教授等。1991 年获南京航空航天大学学士学位;1995 年获中国科学院光学精密机械与物理研究所博士学位。1995 年至 1997 年,在清华大学从事博士后研究;1997 年至 1998 年,在明尼苏达大学电子工程系做博士后副研究员。1998 年至 1999 年,在日本计量技术国家实验室做 STA 研究员。1999 年至 2003 年,在美国路易斯安娜理工大学的电子工程系和微加工技术研究所任助理教授。目前主要研究方向包括微米与纳米集成加工技术、微机电系统以及聚合物电子和光电子器件。发表相关学术论文 100 余篇,申请美国专利多项。培养博士毕业生 6 名,硕士毕业生 7 名。